Supporting Information:

1. Quantum chemistry calculations and the reaction paths

Quantum chemistry calculations of the global-minimum structures GM_i and transition states $TS_{i,i+1}$ of all molecular rotors B_{11}^-, B_{13}^+, B_{15}^+, and B_{19}^-, along with their energies and normal modes, were accomplished at the PBE0/6-311+G* level of theory, using the Gaussian 09 suite of programs.[39] The results are in agreement with those of Refs. 15-21. The barrier heights for B_{11}^-, B_{13}^+, B_{15}^+, and B_{19}^- at this level are 224.3, 104.5, 454.2, and 6.4 $\mathrm{hc}\cdot\mathrm{cm}^{-1}$, respectively. The present rotational/pseudo-rotational cyclic reaction path (rpr-CRP) passes through all the global-minimum structures $GM_1, GM_2, \ldots$, and through all transition states $TS_{1,2}, TS_{2,3}, \cdots$, see Fig. 1f. The motion along the reaction path correlates with the corresponding in-plane lowest-frequency normal modes of all GM_i and the imaginary-frequency normal modes of all $TS_{i,i+1}$; see Figs. 1g and 1h. All the GM_i configurations are equivalent. In the molecular ground state they are populated, therefore, with equal probabilities, as shown in Figs. 2 and 4e-4h. This is a general property, irrespective of the definition of the rpr-CRP.

As an example, we now define the rpr-CRP of B_{11}^-. According to Fig. 1, the nuclei of the wheel of B_{11}^- rotate (almost) on a circle, and each nucleus of the outer bearing moves along equivalent periodic orbits (nearly ellipsoidal). The mean angular velocities of the nuclei of the bearing are twice as fast compared to the nuclei of the wheel, that is, they run a full cycle around their ellipses when the wheel moves only half a circle. It is therefore convenient to define the rotational angle φ such that the wheel rotates with angular velocity $\dot{\varphi}$, while each nucleus of the outer bearing moves with mean angular velocity $2\dot{\varphi}$. The corresponding nuclear coordinates are

$$x_k = x_{k0} + a\cdot\cos(\varphi_{k0} + 2\varphi), \tag{S1a}$$
$$y_k = y_{k0} + b\cdot\sin(\varphi_{k0} + 2\varphi), \tag{S1b}$$
$$z_k = 0, \tag{S1c}$$

where $k = 1, \ldots, 9$ for the outer bearing, and

$$x_i = x_{i0} + R\cdot\cos(\varphi_{i0} + \varphi), \tag{S2a}$$
$$y_i = y_{i0} + R\cdot\sin(\varphi_{i0} + \varphi), \tag{S2b}$$
$$z_i = 0, \tag{S2c}$$

for the nuclei of the wheel, $i = 1, 2$. According to Fig. 1 we have

$$\varphi_{k0} = (k-1)\cdot 40^{\circ}, \qquad k = 1,\mathsf{L}\ ,9 \tag{S3a}$$

$$\varphi_{i0} = (i-1)\cdot 180^{\circ}, \qquad i = 1,2 \tag{S3b}$$

Thus the rpr-CRP is well described in terms of the rotational angle φ, ranging from 0° to 360°. One can also say that the rpr-CRP is mapped on φ. The structures of 18 equivalent GM_i yield the parameters for the inner circle and for the outer ellipses,

$$R = 0.892\ \text{Å}, \tag{S4a}$$

$$a = 0.423\ \text{Å}, \tag{S4b}$$

$$b = 0.159\ \text{Å}. \tag{S4c}$$

We close this section with a caveat, i.e., the interpretations of the results depends on the reference frame. In the laboratory frame, the light compact inner wheel rotates much faster than the heavy outer bearing - this is a consequence of the order of magnitude difference of the small and large moments of inertia of the molecular wheel and the bearing, respectively. For example, if the molecular wheel of B_{11}^{-} makes a full cycle ($360°$) in the laboratory frame, then its bearing counter-rotates by just $14°$, i.e. the bearing stands almost still (see equations (S9a) and (S9b) for the corresponding moments of inertia). In this work, we start by considering rotations of the planar boron clusters in the laboratory frame, but then we prefer it to switch to the frame where the inner wheel rotates with respect to the outer bearing. Switching frames is ubiquitous in every day's life, for example one may view the sun as rotating around the earth, or vice versa.

2. The effective moment of inertia

The Hamiltonian for the one dimensional rpr-CRP model can be written as

$$H = -\frac{\mathsf{h}^2}{2I_{\text{eff}}}\frac{\partial^2}{\partial\varphi^2} + V(\varphi). \tag{S5}$$

According to Ref. 22, the effective moment of inertia I_{eff} can be obtained as

$$I_{\text{eff}} = I_{\text{rot}} + I_{\text{pseudo}}, \tag{S6}$$

where

$$I_{\text{rot}} = \frac{I_{\text{w}}\cdot I_{\text{b}}}{I_{\text{w}} + I_{\text{b}}}, \tag{S7}$$

is the reduced moment of inertia of the rotating wheel in its bearing (analogous to the reduced mass of two particles, e.g., the atoms of a diatomic molecule), and

$$I_{\text{pseudo}} = 9\times 2^2 \times I_{\text{p}} \tag{S8}$$

accounts for the pseudo-rotation of the nine nuclei of the bearing. The factor 2^2 accounts for the fact that the angular velocity of each nucleus of the bearing is twice as fast as the wheel.[22] Here I_w, I_b and I_p are the moments of inertia of the inner wheel, of the outer bearing, and of the individual nuclei running along their ellipsoidal orbitals, respectively, which amount to

$$I_w = 2 \cdot m_B \cdot R^2 = 1.59\ m_B \cdot Å^2 = 17.5\ u \cdot Å^2, \tag{S9a}$$

$$I_b = \sum_{k=1}^{9} m_B \cdot (x_{k0}^2 + y_{k0}^2) = 41.29\ m_B \cdot Å^2 = 454.6\ u \cdot Å^2, \tag{S9b}$$

$$I_p = \frac{1}{2} m_B \cdot (a^2 + b^2) = 0.1021\ m_B \cdot Å^2 = 1.124\ u \cdot Å^2. \tag{S9c}$$

The above values are obtained using $m_B = 11.01$ u and the parameters in equation (S4). Combining equations (S6) to (S9) we have

$$I_{eff} = (16.85 + 40.46)\ u \cdot Å^2 = 57.3\ u \cdot Å^2. \tag{S10}$$

Now we introduce an alternative way to the effective moment of inertia I_{eff}. According to Figs. 1a, 1b, 1g, 1h, the motions along the rpr-CRP correlate with the in-plane lowest-frequency normal mode of each GM_i, as well as the imaginary-frequency normal mode for crossing each $TS_{i,i+1}$. The frequencies of the two modes are

$$\nu_{low} = \omega_{low} / 2\pi = 148.7\ c \cdot cm^{-1}, \tag{S11a}$$

$$\nu_{im} = \omega_{im} / 2\pi = i \times 143.2\ c \cdot cm^{-1}, \tag{S11b}$$

respectively, at the PBE0/6-311+G* level.

The fact $|\nu_{low}| \approx |\nu_{im}|$ supports the simple periodic model potential

$$V(\varphi) = \frac{1}{2} V_b \cdot (1 + \cos(18\varphi)), \tag{S12}$$

with 18 equivalent potential minima. The frequencies ω_{low} and ω_{im} are related to the force constants k_{GM} at the potential minima and k_{TS} at the potential maxima, respectively. Calculating the second order derivative of equation (S12),

$$k_{GM} = I_{eff,GM} \cdot \omega_{low}^2 = \frac{\partial^2 V}{\partial \varphi^2}|_{min} = \frac{1}{2} V_b \cdot 18^2, \tag{S13a}$$

$$k_{TS} = I_{eff,TS} \cdot (\omega_{im} / i)^2 = \frac{\partial^2 V}{\partial \varphi^2}|_{max} = -\frac{1}{2} V_b \cdot 18^2. \tag{S13b}$$

Using the results of equation (S11) and $V_b = 224.3\ \mathrm{hc\cdot cm^{-1}}$, we obtain

$$I_{\mathrm{eff,GM}} = 55.4\ \mathrm{u\cdot Å^2}, \tag{S14a}$$

$$I_{\mathrm{eff,TS}} = 59.7\ \mathrm{u\cdot Å^2}, \tag{S14b}$$

at the PBE0/6-311+G* level. The mean value is

$$I_{\mathrm{eff,m}} = \frac{1}{2}(I_{\mathrm{eff,GM}} + I_{\mathrm{eff,TS}}) = 57.5\ \mathrm{u\cdot Å^2}, \tag{S15}$$

in very good agreement with the value of $I_{\mathrm{eff}} = 57.3\ \mathrm{u\cdot Å^2}$ derived in equation (S10).

3. Quantum mechanical calculations

The wave functions $\psi_v(\varphi)$ and energies E_v representing the rotating wheel in the pseudo-rotating bearing of B_{11}^- are obtained as solutions of the time independent Schrödinger equation (TISE)

$$H(\varphi)\psi_{\mathrm{v}}(\varphi) = E_{\mathrm{v}}\psi_{\mathrm{v}}(\varphi), \tag{S16}$$

with periodic boundary conditions, $\psi_v(0) = \psi_v(2\pi)$. Converged results for the 36 states with the lowest energies were obtained by expanding the wave function $\psi_v(\varphi)$ in terms of 721 periodic basis functions $\frac{1}{\sqrt{2\pi}}\mathrm{e}^{(i\cdot k\cdot\varphi)}$, $k = -360, -359, \cdots, +360$.

The rotational/pseudo-rotational energy spectrum of B_{11}^- displays band structure, with successive groups of 18 states forming an energy band. In each band, the lowest and highest energy levels are non-degenerate, and the remaining 16 energy levels are all doubly degenerate, in accord with the quantum mechanical $D_{9\mathrm{h}}$ symmetry of B_{11}^-. The lowest 36 energy levels (two energy bands) are compiled in Table S1 and illustrated in Fig. 2. The zero point energy of 65.4 $\mathrm{cm^{-1}}$ is smaller than the value of the harmonic approximation at the PBE0 level ($0.5\nu_{\mathrm{low}} = 74.3\ \mathrm{c\cdot cm^{-1}}$), due to the anharmonicity of the motions along the rpr-CRP.

Table S1: Quantum numbers and energies of the lowest 36 rotational/pseudo-rotational states of B_{11}^-

Quantum number	Energy (hc·cm^{-1})	Quantum number	Energy (hc·cm^{-1})
0	65.4	18	171.0
1	65.5	19	171.6
2	65.5	20	171.6
3	65.7	21	173.1
4	65.7	22	173.1
5	65.9	23	175.6
6	65.9	24	175.6
7	66.3	25	179.0
8	66.3	26	179.0
9	66.6	27	183.1
10	66.6	28	183.1
11	67.0	29	187.5
12	67.0	30	187.5
13	67.3	31	191.9
14	67.3	32	191.9
15	67.5	33	195.4
16	67.5	34	195.4
17	67.5	35	196.7

4. Quantum dynamics simulation

Quantum dynamics simulations of the planar all-boron rotors represent the rotating wheels in pseudo-rotating bearings in terms of the time-dependent wave functions $\psi(\varphi,t)$, which are evaluated as solutions of the time-dependent Schrödinger equation (TDSE)

$$\mathrm{i}\,\mathrm{h}\frac{\partial}{\partial t}\psi(\varphi,t) = H(\varphi)\ \psi(\varphi,t)\ , \tag{S17}$$

subject to the initial conditions

$$\psi(\varphi,0) = \psi_{\text{init}}(\varphi) = \sum_{v} c_v \psi_v(\varphi)\ , \tag{S18}$$

Equation (S18) expands the initial wave function $\psi_{\text{init}}(\varphi)$ in terms of the eigenfunctions $\psi_v(\varphi)$ of the rotor, which have been obtained as results of the TISE (S16), together with the eigenenergies E_v. The solution of the TDSE (S17) then is

$$\psi(\varphi,t) = \sum_{v} c_v\ e^{-iE_v t/\mathrm{h}}\psi_v(\varphi)\ . \tag{S19}$$

Here we evaluate the dynamics of the model rotor B_{11}^- for two different initial conditions, $\psi_{\text{init}}(\varphi) = \psi_{\text{local},0}(\varphi)$ and $\psi_{\text{local},1}(\varphi)$, assuming initial localization in a single potential well that supports a single global minimum, specifically in its ground (local,0) or first excited (local,1) states; the corresponding expansions (S18), (S19) are in terms of the eigenfunctions of the lower and upper bands, respectively. These initial states are, of course, not eigenstates of the rotors. In other words, they are non-stationary. The resulting time evolutions correspond to rotations/pseudo-rotations from the single initial global minimum structure say GM_i via the transition states $TS_{i,i+1}$ or $TS_{i-1,i}$ to the neighboring GM_{i+1} or GM_{i-1}, and from there either to the next neighbouring GM_{i+2} or GM_{i-2}, or back to GM_i, and so on. This is illustrated by the time-evolutions of the densities in Figs. 4 and S1,

$$\rho(\varphi,t) = \sum_v c_v^2 \psi_v^2(\varphi) + \sum_{v \neq w} c_v c_w \psi_v(\varphi)\psi_w(\varphi)\cos[(E_v - E_w)t/\mathrm{h}] \ . \qquad \text{(S 20)}$$

The initial localized wave functions thus delocalize such that they penetrate from the initial potential well into the neighboring ones, then into the next-neighboring ones, and so on. At the same time, the populations of the initial potential well decrease, to the benefit of populations of the other potential wells. Since the rotation/pseudo-rotation is cyclic, the frontier lobes of the spreading wave functions reach again the initial well, after some time. Here they may interfere constructively, which corresponds to some re-population of the initial global minimum structure, or the initial potential. Quantitatively, the population of the initial state is calculated (using Dirac notation $\psi(\varphi,t) = \langle \varphi | \psi(\mathrm{t}) \rangle$) as

$$P(t) = \left| \langle \psi(0) | \psi(t) \rangle \right|^2 = \sum_v c_v^4 + \sum_{v \neq w} c_v^2 c_w^2 \cos[(E_v - E_w)t/\mathrm{h}] . \qquad \text{(S 21)}$$

A re-population of the initial global minimum structure appears as temporal peak in $P(t)$. The phenomenon is well known for other cyclic systems - they may be called "revivals of the initial state"; see e.g. Ref. 37. Revival patterns in quantum mechanics are often quite complex: One typically observes some "partial revivals" before the system exhibits a more significant revival at revival time τ. Here this does not necessarily mean a complete revival ($P(\tau) = 1$), but in any case the peak $P(\tau)$ sticks out of smaller partial revivals. In the present case, the time it takes from t = 0 to the time $t = \tau$ of the first "significant revival" characterizes the period of rotation/pseudo-rotation of the rotor. The period depends, of course, on the initial preparation of the system. Below we shall call these periods τ_{lower} and τ_{upper}, corresponding to the initial states $\psi_{\text{local},0}$ and $\psi_{\text{local},1}$ that are expanded in terms of the eigenfunctions of the lower and upper bands, respectively.

The resulting time evolutions $P(t)$ of the populations of the initial global minimum structure prepared in states $\psi_{\text{local},0}$ and $\psi_{\text{local},1}$ are shown in Figs. 4 and S1, respectively. The revival patterns yield the rough estimates of the rotational/pseudo-rotational periods, $\tau_{\text{lower}} \approx 127$ ps and $\tau_{\text{upper}} \approx 8$ps. Apparently, excitation of the planar all-boron rotor from its single initial global minimum structure in the ground state to the first excited state

speeds up rotation of the inner wheel in its pseudo-rotating outer bearing, with corresponding decrease of the period. This decrease corresponds to the increasing spacings of the energy levels of the broader upper band, compared to the narrow lower band. Note that this is an intrinsic property of the rotor. Quantum dynamics simulations of selective uni-directional rotations/pseudo-rotations driven by external circularly polarized IR laser fields, somewhat analogous to the classical trajectory simulations of Ref. 21, will be published separately.

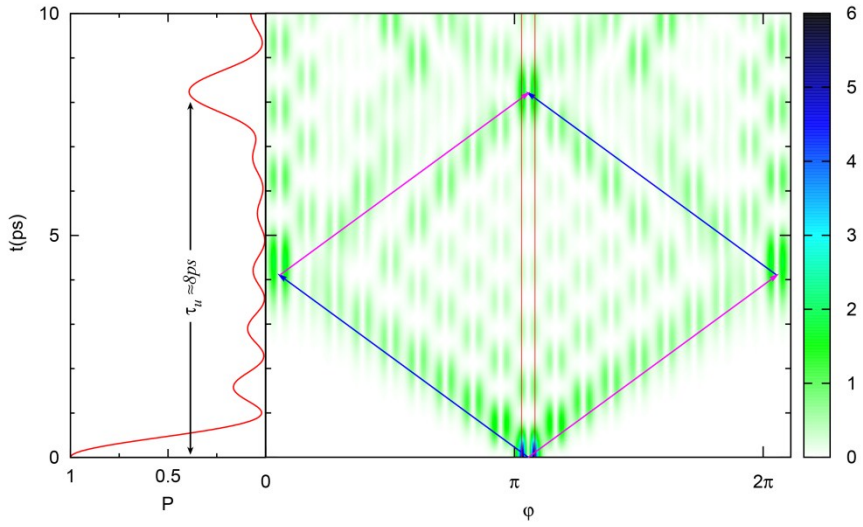

Fig. S1. Same as Fig. 4, but for the first excited state.

References:

39. M. J. Frisch, G. W. Trucks, H. B. Schlegel, G. E. Scuseria, M. A. Robb, J. R. Cheeseman, G. Scalmani, V. Barone, B. Mennucci, G. A. Petersson, H. Nakatsuji, M. Caricato, X. Li, H. P. Hratchian, A. F. Izmaylov, J. Bloino, G. Zheng, J. L. Sonnenberg, M. Hada, M. Ehara, K. Toyota, R. Fukuda, J. Hasegawa, M. Ishida, T. Nakajima, Y. Honda, O. Kitao, H. Nakai, T. Vreven, J. A. Montgomery, J. E. Peralta, F. Ogliaro, M. Bearpark, J. J. Heyd, E. Brothers, K. N. Kudin, V. N. Staroverov, R. Kobayashi, J. Normand, K. Raghavachari, A. Rendell, J. C. Burant, S. S. Iyengar, J. Tomasi, M. Cossi, N. Rega, J. M. Millam, M. Klene, J. E. Knox, J. B. Cross, V. Bakken, C. Adamo, J. Jaramillo, R. Gomperts, R. E. Stratmann, O. Yazyev, A. J. Austin, R. Cammi, C. Pomelli, J. W. Ochterski, R. L. Martin, K. Morokuma, V. G. Zakrzewski, G. A. Voth, P. Salvador, J. J. Dannenberg, S. Dapprich, A. D. Daniels, Ö. Farkas, J. B. Foresman, J. V. Ortiz, J. Cioslowski, D. J. Fox, *Gaussian 09, Revision D.01, Gaussian Inc., Wallingford, CT*, 2010.